Applied Thermal Engineering 67 (2014) 201–213

Contents lists available at ScienceDirect

Applied Thermal Engineering

journal homepage: www.elsevier.com/locate/apthermeng

Numerical modeling of flow through an industrial burner orifice

L.C.B.S. Reis [a,b,c], J.A. Carvalho Jr. [a,*], M.A.R. Nascimento [d], L.O. Rodrigues [d], F.L.G. Dias [d], P.M. Sobrinho [a]

[a] Universidade Estadual Paulista, Campus de Guaratinguetá, Guaratinguetá, SP, Brazil
[b] Fundação Oswaldo Aranha, Volta Redonda, RJ, Brazil
[c] Usina Presidente Vargas, Companhia Siderúrgica Nacional, Volta Redonda, RJ, Brazil
[d] Universidade Federal de Itajubá, Itajubá, Brazil

HIGHLIGHTS

- Numerical modeling of natural gas flow through an industrial burner was performed.
- Standard, RNG, Realizable $k-\varepsilon$, and Reynolds Stress Model (RSM) have been used.
- The considered models represent the experimental conditions.

ARTICLE INFO

Article history:
Received 7 November 2013
Accepted 14 February 2014
Available online 4 March 2014

Keywords:
Industrial combustion
Process simulation
Numerical analysis
Industrial burner
Natural gas

ABSTRACT

This paper presents numerical modeling of a turbulent natural gas flow through a non-premixed industrial burner of a slab reheating furnace. The furnace is equipped with diffusion side swirl burners capable of utilizing natural gas or coke oven gas alternatively through the same nozzles. The study is focused on one of the burners of the preheating zone. Computational Fluid Dynamics simulation has been used to predict the burner orifice turbulent flow. Flow rate and pressure at burner upstream were validated by experimental measurements. The outcomes of the numerical modeling are analyzed for the different turbulence models in terms of pressure drop, velocity profiles, and orifice discharge coefficient. The standard, RNG, and Realizable $k-\varepsilon$ models and Reynolds Stress Model (RSM) have been used. The main purpose of the numerical investigation is to determine the turbulence model that more consistently reproduces the experimental results of the flow through an industrial non-premixed burner orifice. The comparisons between simulations indicate that all the models tested satisfactorily and represent the experimental conditions. However, the Realizable $k-\varepsilon$ model seems to be the most appropriate turbulence model, since it provides results that are quite similar to the RSM and RNG $k-\varepsilon$ models, requiring only slightly more computational power than the standard $k-\varepsilon$ model.

1. Introduction

The search for higher energy efficiency of industrial scale combustion furnaces and burners to obtain fuel savings has demanded experimental studies that are complemented with Computational Fluid Dynamics simulations. Industrial burners operate in non-premixed conditions for safety reasons. Fuel and oxidizer enter separately into the combustion furnace and are then mixed and burnt through continuous diffusion only after being discharged from the orifice. Gas fuel is supplied through the orifice and combustion air enters from the surroundings so that the gas can only be burnt within a certain distance from the orifice. Burner designers must determine the correct area of the fuel orifice. For a determined orifice size, there is a specific fuel pressure in order to have the right mix with the combustion air. High fuel pressure can result in soot or flame impingement and low fuel pressure can result in air excess and may not allow the achievement of the required furnace heat load.

Combustion modeling studies have been intensely developed during the last 20 years and the phenomena of flame diffusion is usually treated downstream from the orifice burner. Great

* Corresponding author. Av. Ariberto Pereira da Cunha, 333, Departamento de Energia, Guaratinguetá, SP CEP 12516-410, Brazil.
E-mail addresses: joao@feg.unesp.br, joao.a.carvalho.jr@pesquisador.cnpq.br (J.A. Carvalho).

http://dx.doi.org/10.1016/j.applthermaleng.2014.02.036
1359-4311/

Nomenclature

A	geometrical orifice area (m^2)
c	speed of sound (m s^{-1})
C_d	discharge coefficient of the orifice (dimensionless)
d	nozzle diameter (m)
D	pipe diameter upstream of the nozzle (m)
f	friction factor (dimensionless)
K	pressure drop coefficient for losses of fittings (dimensionless)
k	turbulent kinetic energy per unit mass (m^2 s^{-2})
k	ratio of specific heats of the fuel (dimensionless)
L	length of pipe (m)
$\dot{m}$	mass flow rate (kg s^{-1})
MW	molecular weight (kg $kgmol^{-1}$)
P_1	fuel pressure at upstream from the nozzle (N m^{-2})
P_2, P_b	fuel pressure at downstream from the nozzle (N m^{-2})
Q	volumetric flow rate (m^3 s^{-1})
$\overline{R}$	universal gas constant (J $kgmol^{-1}$ K^{-1})
T	temperature (K)

Greek symbols

α	port angle in a burner nozzle
β	ratio of orifice diameter to pipe diameter
Δ	difference in a quantity
ε	turbulent energy dissipation

Subscripts

1	nozzle entrance
2	nozzle exit

Abbreviations

ICEM CFD	a meshing software
CFD	computational fluid dynamics
DO	discrete ordinate method
EDM	Eddy-Dissipation Model
LFM	Laminar Flamelet Model
PDF	Probability Density Function
RSM	Reynolds Stress Model
WI	Wobbe Index
WSGGM	weighted sum of gray gases model

attention has been given to investigating the interaction of turbulence combustion and its consequences, including deciding which turbulence model is the most appropriate depending on the specificity of the application. Usually the burner orifice modeling does not take part of the analysis. However, for industrial burners it is very important to have information about the pressure upstream from the burner, since changes in fuel chemical composition can be compensated by altering fuel pressure. Burner nozzles are designed for a certain orifice discharge coefficient obtained from experimental measurements. This coefficient is defined as the ratio of actual flow to the maximum theoretical flow and is normally obtained using empirical correlations based on experimental data, derived under controlled laboratories conditions.

The present paper reports a numerical analysis identifying the most appropriate turbulence model to simulate the flow through an industrial burner orifice, establishing comparisons with the best turbulence models for some combustion applications. Flow rate and pressure at burner upstream were validated by experimental measurements. The results indicate that the standard, RNG, and Realizable k–ε models and Reynolds Stress Model (RSM) satisfactorily represent the experimental conditions. However, the Realizable k–ε model seems to be the most appropriate turbulence model, since it provides results that are quite similar to the RSM and RNG k–ε models, requiring only slightly more computational effort than the standard k–ε model. The industrial burner is a non-premixed swirl burner from the preheating zone of slab reheating furnaces. It is from Usina Presidente Vargas, a major steelworks that belongs to Companhia Siderúrgica Nacional (CSN), located in the state of Rio de Janeiro, Brazil.

2. Literature review

Few attempts have been made to simulate turbulent combustion with burner orifice flow pattern. Indeed, most of the numerical and experimental works have studied orifice meters, and a few have studied hydraulic orifices. The following presents a list of published literature of correlated papers. The quality of the simulations for orifice flow and the choice of turbulent models are discussed.

Experiments on orifice fluid flow measurements were simulated [1] using data provided by others [2,3]. CFD simulations were validated through pressure drop and energy balance measurements using water as fluid. The standard k–ε turbulence model was used. A comparison of the numerical and experimental results revealed that experimental data closely agreed with CFD predictions.

Experimental discharge coefficients for flow meters, including orifice plate flow meters, were obtained in order to validate numerical results at low Reynolds numbers [4]. The Realizable k–ε model was used for turbulence closure. The intent of the study was to present characteristic curves to enable users to better understand the relative differences expected at low Reynolds numbers.

CFD was applied to numerically predict the calibration coefficient of orifice meters in order to ease the laborious experimental procedure of calibration [5]. The methodology satisfactorily predicted the discharge coefficients.

The flow through a circular orifice was investigated using CFD and two turbulence modeling techniques [6]. The standard k–ε model and the Reynolds Stress Model (RSM) were employed. It was found that the results agreed well with experimental data. However, the RSM was more accurate in the downstream orifice region than the k–ε model.

A numerical study was conducted to evaluate effects of flow through a simple orifice [7]. The main recommendations are that the grid spacing must be 0.1% of pipe diameter upstream of the plate and the use of high-order differencing schemes in order to calculate pressure loss correctly. The standard k–ε model was used. It agreed sufficiently with experimental data, but the authors recommended the use of other turbulence models or modification of the k–ε model to improve performance.

Another study [8] proposed to relax the square root relation commonly used by international standards to determine the flow rate through a specific discharge coefficient value. The resulting power law relation was shown to improve accuracy. In addition to the experimental data, evidence was also obtained by performing numerical simulations. The standard k–ε turbulence model was used.

A single empirical formula to model the flow through hydraulic orifices was proposed [9]. It makes use of a linear relation for small pressure differences and the conventional square root law for turbulent conditions. Simulation results have proved to be accurate.

The effect of contaminated orifice plates on the discharge coefficient was investigated [10]. Experimental work was

conducted simulating contamination by sticking circular metal discs. Computational fluid dynamics was used to assist interpretation and had good agreement with experiments.

Several works have been made employing computational fluid dynamics simulations of flow in non-premixed burners. Those works were made to investigate or predict flame properties and combustion flow fields [11], pollutant emissions [12–19] and the mechanism of flame stability [13]. Combustion modeling has been performed using several turbulence models, the standard k–ε [11,14–22], Reynolds Stress Model [11,12,16,22] and Realizable k–ε [14,21]. With respect to combustion models for non-premixed combustion for conventional flames, the most used are the Probability Density Function/Laminar Flamelet Model (PDF/LFM) [12,23] and the Eddy Dissipation Model (EDM) [1,13,15,17,18,20–22]. The Eddy Dissipation Concept (EDC) [14,16] is mainly used for flameless combustion. EDM was chosen for this study. The quality of combustion modeling simulations using EDM and the choice of turbulence models are discussed in the following.

Modeling of non-premixed swirl burner flows was investigated using RSM and standard k–ε turbulence models [11]. The results agreed well with experimental data. Results of computational and experimental investigations of a turbulent asymmetric vortex flame were presented [13]. The three-dimensional reacting flow fields were described using EDM and the modified standard k–ε turbulence model, called R_ε/k–ε. The mechanism of flame stability and interaction with the forced vortex field was discussed. The effect of increasing the intensity of turbulence in the air stream on NO_x and soot formation in turbulent methane diffusion flames was investigated [18]. The interaction between turbulence and combustion in the flame field was modeled using the standard k–ε and EDM models. It was found that increased intensity of free stream turbulence in the air supply results in a significant reduction in NO formation. Reduction of soot formation was also found. The implementation of EDM in an OpenFOAM CFD toolbox was discussed [20]. The code was validated by modeling a confined non-premixed methane jet flame using the standard k–ε turbulence model. The predictions were compared with published experimental results and the ANSYS Fluent predictions. The results showed that the predictions agreed with the experimental results. The performance of four turbulence models in modeling a co-flowing turbulent diffusion methane/air flame based on EDM was analyzed [21]. The method of computing the dissipation rate of turbulent kinetic energy is considered crucial to accurately express reaction rate. It was shown that the Realizable k–ε turbulence model is better than the other models, including the standard k–ε model. A numerical study of the swirl effect on a coaxial jet combustion diffusion flame was presented [22]. EDM and the standard k–ε turbulence model were used. The results showed that EDM agreed well with experimental data.

3. Experimental setup

The primary function of the hot rolling furnace is to reheat semi-finished steel slabs to temperatures of about 1250 °C. The interior of the furnace is divided into seven zones for temperature control: preheat, top-and-bottom; heating, top-and-bottom; and soak, top-and-bottom, with two zones for top soaking. All zones can burn natural gas or coke oven gas with preheated combustion air by means of recuperative heat exchangers. The preheating zone of the reheating furnace is equipped with six side swirl burners, three on each side of the furnace. Each burner has a thermal power of 4360 kW. The walking-beam reheating furnace has inner dimensions of 34,806 × 11,580 × 3,800 mm^3 (length × width × height).

Fig. 1 shows a longitudinal cross-section view of the furnace with an indication of the burner used in this study. The skids are not shown in this view. The computational domain considered is crosshatched in Fig. 1. Its perspective view is detailed in Fig. 2a. It comprises the region surrounding the flame up to the limits of the neighbor burner at right, which defines a surface of flue gas outlet in the direction of the natural draft stack; the incoming flue gases from bottom heating and bottom soaking zones are at the left; the refractory floor is at the bottom; the slab is at the top; the centerline of the furnace is seen as a symmetrical surface, since there is an opposite burner in the same direction; and the casing/refractory wall which is equipped with the burner is shown.

Inside the furnace, the slabs are supported by water-cooled, refractory-coated pipes called “skids”. To minimize the cold spots or “skid marks” left in the slab, the skid spacing changes twice along the furnace. This is the reason for the variation of direction of the skid pipe. There are two independent set of skids, one fixed and one moving, which take turns supporting the slab as it is transported through the furnace by a frame moved by large hydraulic cylinders. The skids also are represented in the numerical model as shown in Fig. 2a. Thus, there are two boundaries of heat absorption: one the skid cooling tubes; and other the slab on the top of the domain. Fig. 2b shows a photograph of the burner portion outside of the furnace.

The BHF.M.10-type swirl configuration preheating zone burners were manufactured by Stein Heurtey. Each burner has eight gas nozzles with diameters of 33 mm, twelve primary air nozzles with diameters of 59 mm which promote air swirl, sixteen secondary air nozzles with diameters of 51 mm, and a heavy oil lance which is not in operation anymore. The burner geometry created on ICEM CFD is shown in Figs. 3a, b and 4a. Fig. 4b shows a side view of the burner.

The furnace operates at atmospheric pressure. Furnace pressure was measured at the boundary surface of the outlet gases using an LD 3000 M pressure gauge (accuracy ± 0.04%; manufacturer: Beta Calibrator-Martel Electronics). Furnace temperatures were measured with type R thermocouples (accuracy ± 1.8 °C; manufacturer: Ecil). Air and gas pressure were measured by betagauge 320 pressure calibrator (accuracy ± 0.075%; Martel Electronics) and Testo 521-1 (accuracy ± 0.2%; manufacturer: Testo). Air flow rate was measured by LD 301-D1 (±0.04%; manufacturer: Smar) and gas flow rate was measured by LD 301-D3 (±0.04%; manufacturer: Smar). Temperature inside the furnace was measured by a thermocouple on the end of a stainless steel lance of 6 m length, placed through the heavy oil nozzle (centerline of the burner) and positioned at 4.5 m distance from the burner wall.

The experimental data that have been taken for the present simulations are considered to be closest to steady state operation. Natural gas was used as the fuel. Its main characteristics are presented on Table 1.

4. Theory

The review of the literature demonstrated that there is little information about turbulence numerical analysis to simulate the flow through an industrial burner orifice. Consequently, this study was performed to analyze the available turbulence models for this type of application.

In order to simulate the steady state flow though the nozzles, the Reynolds-averaged Navier–Stokes equations were solved, including mass conservation, momentum conservation, turbulent kinetic energy and energy dissipation rate equations. Although the domain of analysis is upstream from the beginning of chemical reaction, the complete domain also took the zones with reaction flows into account in order to assure that mass and energy balances were consistent. Conservation for the species transport equation

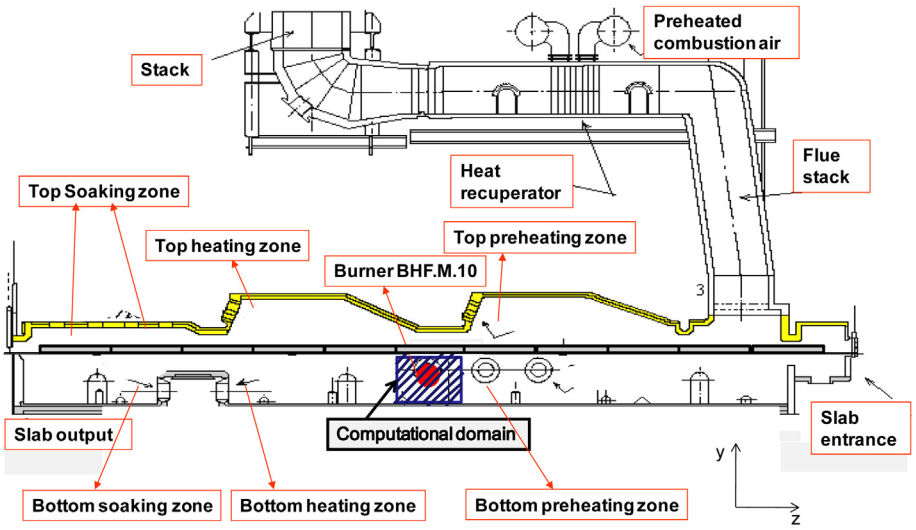

Fig. 1. Longitudinal cross-section of the reheating furnace showing the computational domain.

was considered as well. Those equations were solved for steady state conditions by utilizing FLUENT computational fluid dynamics [24].

5. Computational work

Three dimensional simulations have been carried out for modeling. Several operational conditions were considered, varying the flow rate of natural gas and, consequently, of the combustion air. A furnace sketch showing the polyhedral mesh applied for the whole domain is presented in Fig. 5a and a detailed mesh view of the burner nozzles is shown in Fig. 5b.

Pressure-velocity coupling was accomplished by using SIMPLE (Semi Implicit Pressure Linked Equation) algorithm. The solver used was the "pressure-based segregated", in which the governing equations are solved in sequence. Interpolation of variables to cell faces was performed using a second-order up-winding scheme, except for pressure, which was used the "standard" scheme. The under-relaxation parameters were set to 0.3 for pressure, 0.6 for density, 0.7 for body forces, 0.7 for momentum equations, 0.5 for turbulent quantities, 0.2 for energy and 0.3 for chemical species.

A computational mesh was created for the domain, as shown in Fig. 5a. A refined mesh was used for the burner nozzles as shown in Fig. 5b. Mesh geometries contained on the order of 650,000 cells. A three dimensional tetra-mixed mesh was generated using ICEM CFD and converted to polyhedral cells in FLUENT 12.0.16, the commercial code used to perform the simulations. The skid cooling tubes were entirely incorporated into the simulations. The calculations were performed on a computer with 08 Intel Xeon Quad-core 5420 processors (2.5 GHz/12 MB) and 16 GB RAM, connected to a cluster with 40 cores distributed per a total of 5 computers.

5.1. Turbulent combustion modeling

The standard $k-\varepsilon$ turbulence [25] was used. It is widely validated and it has also been shown to have excellent performance for many relevant industrial flows. However, as the case in point is a swirl burner and the most recommended turbulence modelings in swirling flows are the RNG $k-\varepsilon$, the Realizable $k-\varepsilon$ and the Reynolds stress models, they were also used in the simulation.

Combustion modeling used the Eddy-Dissipation (EDM) model, which considers fast burning, with the overall rate of reaction controlled by turbulent mixing. For cases of non-premixed flames, turbulence slowly convects and mixes fuels and oxidizer into the reaction zones, where they burn very quickly. Combustion proceeds whenever turbulence is present and every reaction has the same turbulent rate, which is used only for one-step or two-step global reactions. Thus, the limitation of the model is that kinetically controlled species as radicals cannot be predicted and intermediate species are neglected. The present work does not concern the prediction of such radicals and the problem being modeled is clearly a fast burning case of high temperature flame, so the EDM is an appropriate model to be used, avoiding the use of multi-step chemical mechanisms based on Arrhenius rates, which can differ for each reaction. Radiative heat transfer was accounted for using the discrete ordinates (DO) method. The absorption coefficient of the flue gas used the domain-based weighted sum of gray gases (WSGGM) model.

Properties of the gas mixture were calculated as follows: density by the ideal gas law and compared to constant density; heat capacities through the mixing law, determined per species through a piecewise-polynomial, enabling composition and temperature dependence. This condition is considered very important for combustion applications to correctly predict flame temperature, since it substantially reduces the peak temperature; molecular viscosity and thermal conductivity by ideal gas mixing law; and mass diffusivity determined by constant dilute approximation coefficient of 2.88×10^{-5} m^2/s.

5.2. Mesh analysis

A mesh study was performed in order to be sure it was sufficiently refined. The results of important parameters such as temperature along the furnace and pressure and velocity through the burner nozzle were analyzed for two different grid sizes. The coarse grid size has 501,853 cells. The fine grid size has 650,000 cells, all the additional cells in the burner domain. The values of the analyzed variables did not change significantly, as shown in Fig. 6, despite a slight reduction in the upstream nozzle pressure for the fine grid (Fig. 6b). This result was very similar to the centerline pressure profile for an orifice meter [1]. The difference with respect to the curve shape is due to the greater length of the orifice for the burner nozzle, 125 mm, which causes a less abrupt pressure drop along its orifice.

(a)

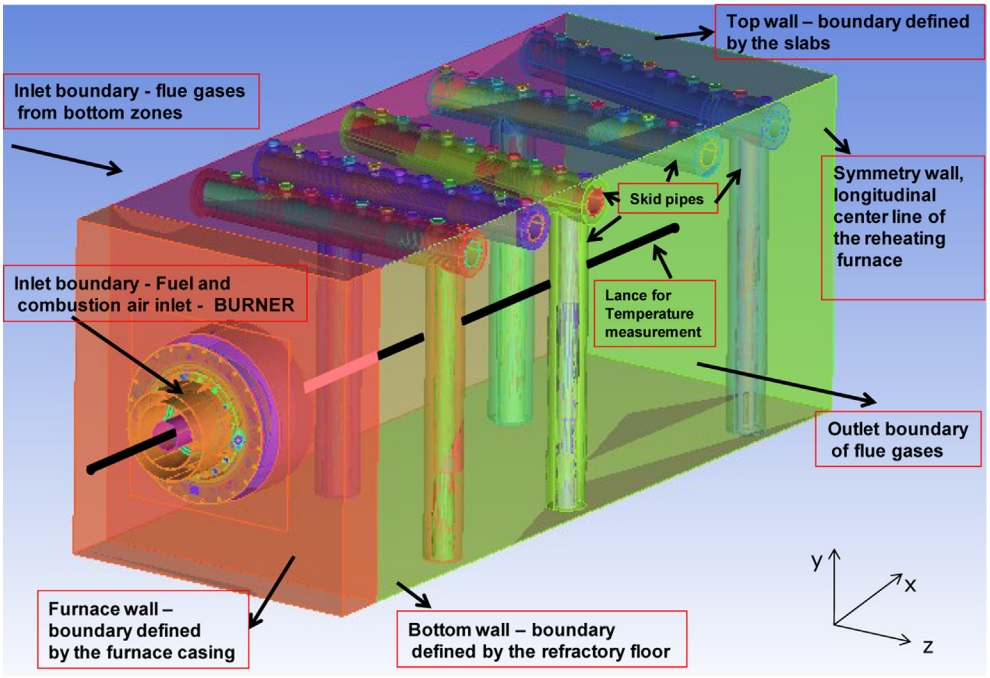

(b)

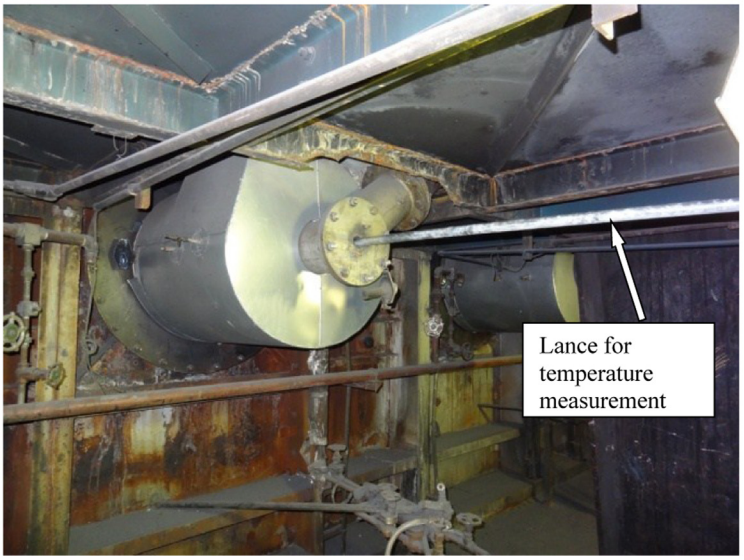

Fig. 2. A perspective view of the computational domain and its boundaries (a), and a front view of the burner outside the furnace (b).

Wall function approach was used to model the near-wall region, since it gives reasonable predictions for high-Reynolds-number wall-bounded flows, which is the case in this work. “Standard wall functions” and “Non-equilibrium wall functions” were used with the aim of comparing the results between those methods, considering that the latter is more appropriate for flows that are characterized by significant pressure gradients, since strong gradients occur in the region of the nozzles. However, the results were the same for both methods.

The dimensionless distances from the wall were checked for each type of nozzle, considering several burner thermal loads. Table 2a presents the results of y^+ for the coarse grid and Table 2b for the fine grid.

Wall roughness effects were taken into account in the turbulent wall-bounded flow. The law of the wall was modified to consider the rough surface of the burner nozzle, as available on FLUENT. It is based on experiments with roughened pipes which indicate that the mean velocity distribution near rough walls has the same slope, but a different intercept, i.e., an additive constant in the log-law. Therefore, a term was introduced in the law-of-the-wall, which is correlated with the physical roughness height. In order to preserve physical significance, the distance

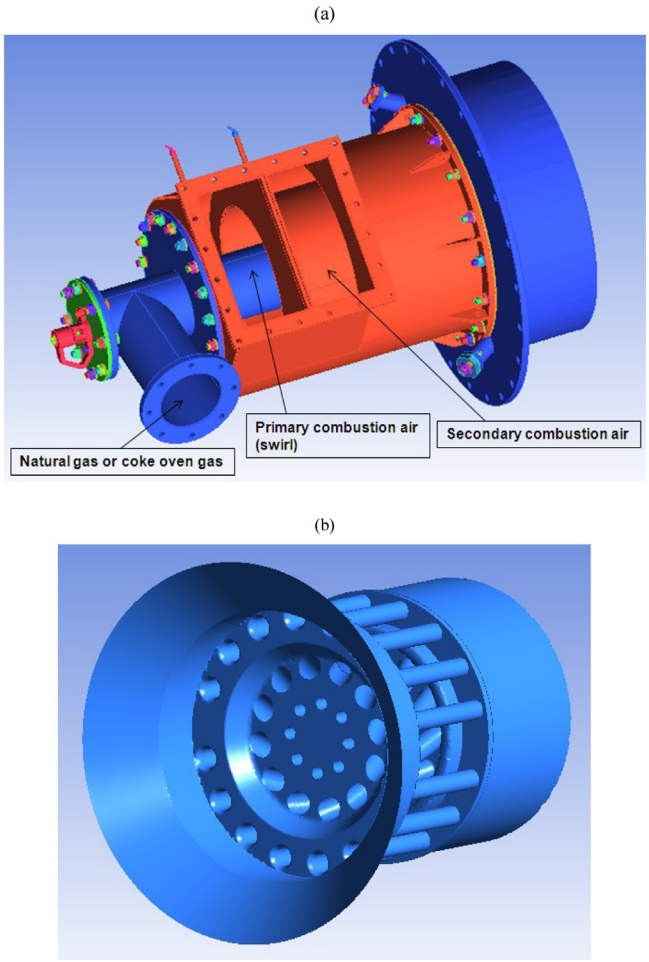

Fig. 3. Perspective view of the BHF.M.10-type burner: external side (a), furnace side (b).

from the wall to the centroid of the wall-adjacent cell was greater than the roughness height.

5.3. Boundary conditions

The domain is made up of the regions shown in Figs. 1 and 2a. The burner orifices are inlet flow boundaries, including fuel, primary and secondary combustion air nozzles. The boundaries inside the furnace are: the refractory floor classified as a wall; the top is the slab, another wall; the symmetry wall, which represents the furnace centerline; flue gas inlet flow boundary is the incoming gases from the bottom heating and soaking zones of the furnace; and flue gas outlet flow which is the sum of the gases from the burner itself and the flue gas inlet flow from the bottom heating and soaking zones. Table 3 summarizes the boundary conditions and the results of mass and energy balances for six different burner heat loads, related to CFD simulations.

5.3.1. Heat transfer at wall boundaries

The slab is a wall boundary at the top of the domain. The calculations were made using a fixed heat flux boundary condition. An average heat flux transmitted to the slab was considered based on the reheating furnace software, which provides the bottom surface and core slab temperature for each axial position inside the furnace, allowing the heat flux to be determined by conduction. The predicted bottom slab temperature was compared to the value provided by the software. The mentioned software is a supervisory system for furnace combustion optimization, provided by the manufacturer Stein Heurtey for furnace operation.

The skid cooling tube was also considered a fixed heat flux boundary condition. Average heat flux transmitted to the skid was based on the total heat absorbed by this system for the entire furnace, which is calculated by measuring the cooling water flow rate and inlet and outlet temperatures.

6. Results and analysis

6.1. Pressure profiles for natural gas

The results are presented in the form of fluid pressure upstream the burner nozzle vs. fluid flow rate. Primarily for natural gas, pressure upstream from the burner nozzle was measured and compared with the numerical predictions, as shown in Fig. 7. The predicted pressure profiles for all turbulence models agreed well with the experimental measurements. However, the results with the standard $k-\varepsilon$ turbulence model indicate that the predicted pressure is somewhat larger than the other turbulence models. Similarly, primary combustion air pressure experimental measurements agreed well with numerical calculations, as shown in Fig. 8. Likewise, the results for standard $k-\varepsilon$ model indicate values slightly higher than the other models. Last, the comparison between secondary combustion air pressure measurements and numerical results also agreed well; however, all turbulence models resulted in identical figures, including the $k-\varepsilon$ model as shown in Fig. 9. This may be attributed to the influence of the swirling flow in the natural gas and primary combustion air nozzles. The secondary combustion air nozzle has less influence on swirling flow, as can be seen in Fig. 10a, b and c, which show the calculated streamlines in the downstream burner region. Fig. 10a shows the calculated streamlines released from natural gas nozzles; Fig. 10b shows the streamlines from primary combustion air nozzles; and Fig. 10c shows the streamlines from secondary combustion air nozzles. As RSM, RNG $k-\varepsilon$ and Realizable $k-\varepsilon$ models account for the effects of swirl, they have greater potential to predict more accurate predictions for swirling flows.

Considering computation time, memory needed and number of iterations to converge, the Realizable $k-\varepsilon$ model is the most appropriate turbulence model to be used for the present application, since it provides quite similar results to RSM and RNG $k-\varepsilon$ models, requiring only slightly more computational power than the standard $k-\varepsilon$ model.

Fig. 11a and b shows the velocity contour and vectors through the nozzles and crossing along the furnace calculated by the simulations. Note the swirl effect caused by primary air that shortens the flame length.

6.2. Compressibility effects

Though the Mach number was less than 0.3, when compressibility effects are considered negligible (Mach values ranging from 0.06 for natural gas burner orifice to 0.21 for secondary air burner orifice in the present study), the present work also explored variable-density flows in the simulation. Since upstream burner pressure is very important in industrial burners, it was verified if constant gas density can really be assumed. Fig. 12 shows that the results were very similar, indicating, as expected, no practical difference between incompressible or compressible flows.

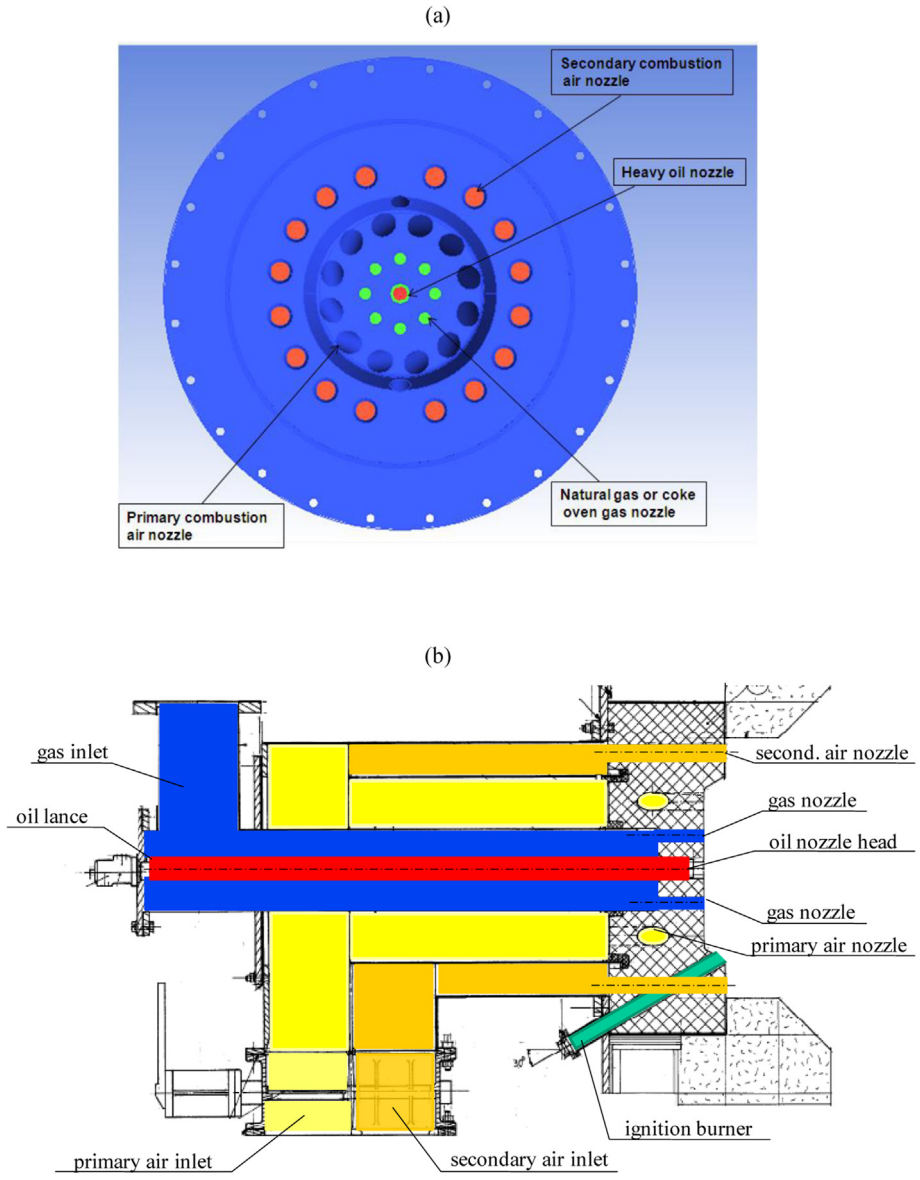

Fig. 4. The BHF.M.10-type burner, furnace side: front view (a), side view (b).

6.3. Discharge coefficient

The discharge coefficient is a parameter for burner design. It is defined as the ratio of the actual mass flow rate of a fluid through a nozzle to the ideal mass flow rate. The dependency of a volumetric flow rate on the pressure drop of the burner can be very accurately calculated for incompressible flows by the well-known equation:

$$Q = C_d A \sqrt{2(p_1 - p_2)/\rho\left(1 - \beta^4\right)}, \quad (1)$$

in which C_d is the discharge coefficient, A is the geometrical orifice area, and β is the ratio between orifice diameter and inlet diameter. Pressure p_1 is upstream from the nozzle and p_2 is downstream from the nozzle. The value of the discharge coefficient for a burner nozzle is usually determined experimentally. Typically, in the burner industry, the discharge coefficient varies from 0.6 to 0.9. This depends on several factors, including the Reynolds number of the fluid in the orifice, length-to-diameter ratio of the orifice, beta ratio (ratio of orifice diameter to entrance pipe diameter), port angle (entering angle of taper) and exit angle, as shown in Fig. 13 [26]. In the case in the study, the orifices have port angle equal to

Table 1
Characteristics of the natural gas used for the simulations (typical for Usina Presidente Vargas).

CH_4	C_2H_6	C_3H_8	nC_4H_{10}	C_5H_{12}	nC_6H_{14}	N_2	CO_2	High heat value (*)	Low heat value (*)	Wobbe Index (**)	Gas density
Molar %								kJ/m^3	kJ/m^3	MJ/m^3	Kg/m^3
89.23	5.73	1.87	0.68	0.20	0.09	0.68	1.52	39,656	35,837	45	0.74

Note: (*) m^3 at 20 °C and 1 atm; (**) WI calculated using the low heat value.

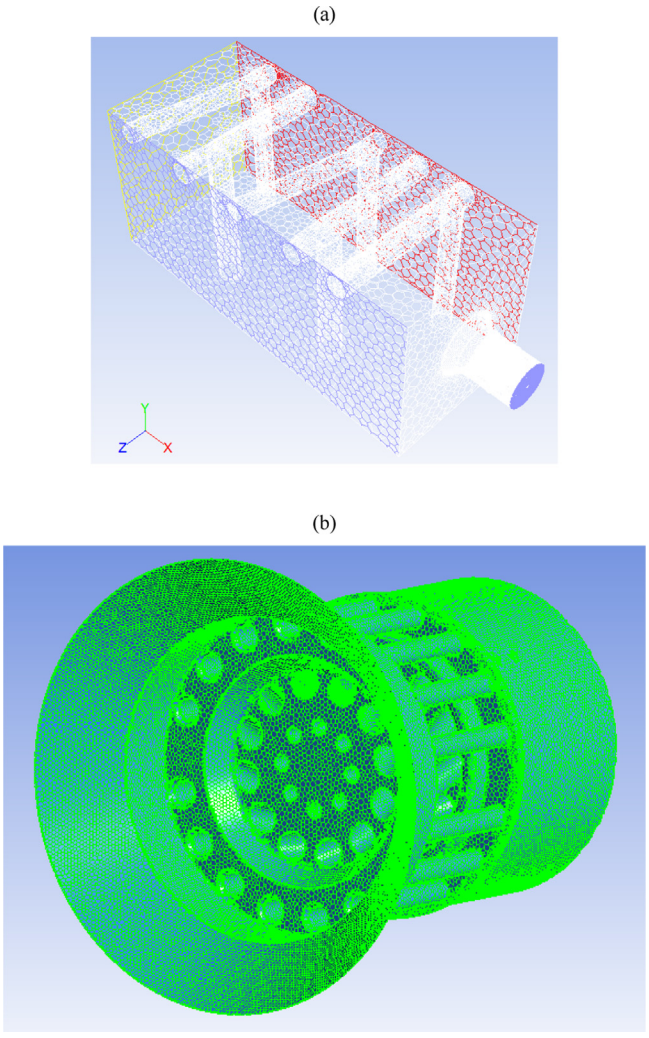

Fig. 5. Polyhedral mesh applied for the entire domain (a); a detailed view of the polyhedral mesh applied for the burner nozzles (b).

90°, exit angle equal to zero degrees, and ratio d/D is 0.2 for natural gas nozzles. Due to these geometry conditions, it is expected that those nozzles have a behavior similar to orifice plates. However, orifice plates have very short L/d ratio (Length/diameter of the nozzle) and the nozzles being analyzed have greater L/d, equal to 3.8 for natural gas nozzles.

Fig. 14 shows the results for calculation of the natural gas nozzle discharge coefficients, using Equation (1) with variable values obtained through the solutions from the numerical simulation. The discharge coefficients are constant at approximately 0.66 for Reynolds Number ranged from 25,000 to 45,000. Lower Reynolds Numbers are not applicable for industrial burners. Larger L/d ratio reduces pressure losses, increasing the discharge coefficient. Experimental results for discharge coefficients of orifice plates [1,27] have constant values of 0.61 for Reynolds Numbers above 10,000. Fig. 14 also shows a comparison with the discharge coefficient formula presented by Colannino [28]. Pressure losses related to skin friction and form drag were calculated by the Idel'cik data [29]:

$$C_d = \sqrt{1/\left(1 + f\frac{L}{D} + \sum_1^n K\right)}, \qquad (2)$$

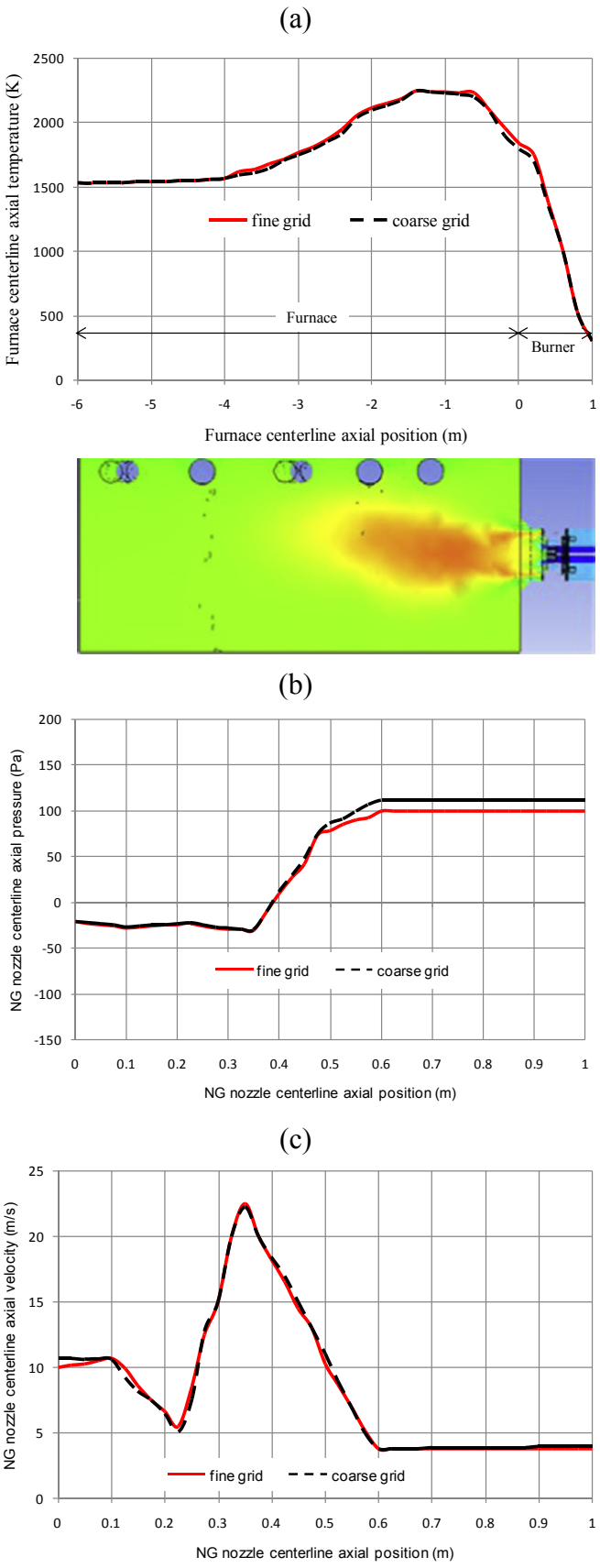

Fig. 6. Effect of mesh size on furnace temperature profile (a), on natural gas nozzle pressure profile (b), and on natural gas nozzle velocity profile (c).

Table 2a
Dimensionless distance from the wall y^+ for coarse grid as a function of burner heat loads and type of nozzle.

Nozzles	Unit	Burner heat load variation					
Natural gas flow rate	kg/s	0.057	0.068	0.080	0.085	0.093	0.101
y^+ natural gas	–	108	110	116	119	125	128
Primary air flow rate	kg/s	0.452	0.542	0.634	0.679	0.739	0.804
y^+ primary air	–	115	141	171	181	211	238
Secondary air flow rate	kg/s	0.507	0.608	0.699	0.761	0.828	0.902
y^+ secondary air	–	140	148	196	214	227	245

Table 2b
Dimensionless distance from the wall y^+ for fine grid as a function of burner heat loads and type of nozzle.

Nozzles	Unit	Burner heat load variation					
Natural gas flow rate	kg/s	0.057	0.068	0.080	0.085	0.093	0.101
y^+ natural gas	–	57	68	80	87	99	110
Primary air flow rate	kg/s	0.448	0.489	0.520	0.610	0.653	0.717
y^+ primary air	–	65	69	72	87	92	103
Secondary air flow rate	kg/s	0.503	0.549	0.584	0.684	0.732	0.804
y^+ secondary air	–	56	60	63	76	80	98

In which f is the friction factor and K represents the losses of bodies or fittings through the flow. The above relation is found using the continuity and energy equations upstream and immediately downstream from the nozzle, including the term for frictional losses. The discharge coefficient is constant around 0.64 regardless the Reynolds number, agreeing well with the numerical values.

Another way to check the results is to use a concept presented by Baukal [26] to calculate the mass flow rate through a nozzle at subsonic flows. The equations are based on the ideal gas law assumptions of ideal flow to calculate the flow rate of fuel through an

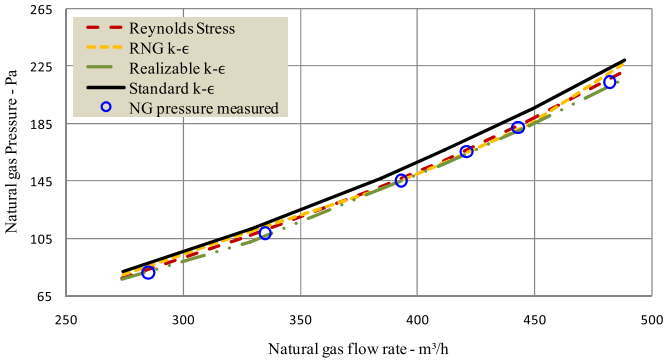

Fig. 7. Comparison between natural gas pressure measurements and predicted profiles for different numerical turbulence models as a function of flow rate.

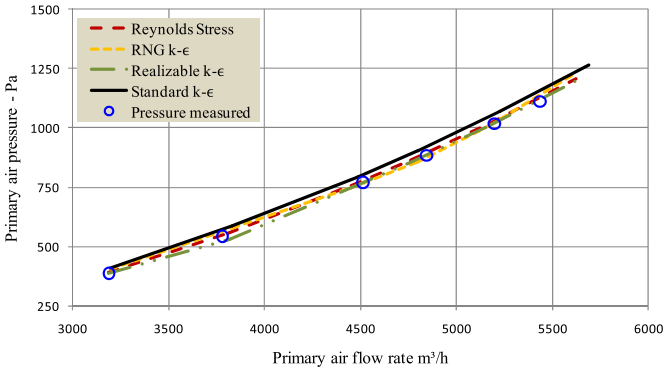

Fig. 8. Comparison between primary combustion air pressure measurements and predicted profiles for different numerical turbulence models as a function of flow rate.

Table 3
Boundary conditions, energy and mass balance results. (a) Boundary conditions of mass flow inlet. (b) Domain outflow and mass/energy balances results.

Case#	Flue gas entrance			Natural gas – burner			Primary air – burner			Secondary air – burner		
	Mass flow rate	Total heat transfer rate	Total sensible heat transfer	Mass flow rate	Total heat transfer rate	Total sensible heat transfer	Mass flow rate	Total heat transfer rate	Total sensible heat transfer	Mass flow rate	Total heat transfer rate	Total sensible heat transfer
	kg/s	kW	kW	kg/s	kW	kW	kg/s	kW	kW	kg/s	kW	kW
1	7.02	−9,080	11,141	0.101	−446	0	0.804	328	328	0.902	368	368
2	7.02	−9,044	11,177	0.093	−409	0	0.739	301	301	0.828	338	338
3	7.02	−9,020	11,202	0.085	−376	0	0.679	277	277	0.761	311	311
4	7.02	−8,998	11,224	0.080	−351	0	0.634	259	259	0.700	285	285
5	7.02	−8,861	11,361	0.068	−300	0	0.542	221	221	0.608	248	248
6	7.02	−8,860	11,361	0.057	−250	0	0.452	185	185	0.507	207	207
	Temperature: 1550 K			Temperature: 300 K; nozzle diameter: 33 mm			Temperature: 691 K; nozzle diameter: 59 mm			Temperature: 691 K; nozzle diameter: 51 mm		

Case#	Flue gas – domain exit									Energy balance – domain		
	Mass flow rate	Mass balance net result	Temperature	Total heat transfer rate	Total sensible heat transfer	Species mass fraction (%)				Heat of reaction source	Total heat transfer rate net result	Total sensible heat transfer rate net result
	kg/s	%	K	kW	kW	O_2	CO_2	H_2O	N_2	kW	%	%
1	8.826	0.01	1600	10,645	−14,782	1.09	15.01	11.42	72.49	4,761	0.22	0.16
2	8.680	0.01	1595	10,602	−14,401	1.09	15.01	11.41	72.49	4,372	−0.04	−0.03
3	8.542	0.03	1592	10,564	−14,043	1.09	15.00	11.41	72.49	4,017	−0.34	−0.20
4	8.431	0.02	1590	10,550	−13,772	1.07	15.02	11.43	72.48	3,754	−0.45	−0.30
5	8.238	0.01	1582	10,481	−13,228	1.08	15.01	11.42	72.49	3,187	−0.03	−0.02
6	8.034	0.02	1568	10,441	−12,631	1.09	15.01	11.41	72.48	2,643	−0.66	−0.21
	Pressure outlet: 10 Pa									Slab heat flux: −1,127 kW (−79.45 kW/m^2); Skid heat flux: −665 kW (−29.00 kW/m^2)		

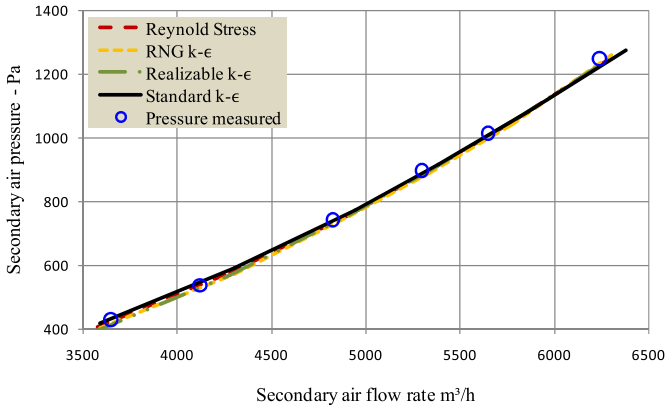

Fig. 9. Comparison between secondary combustion air pressure measurements and predicted profiles for different numerical turbulence models as a function of flow rate.

orifice. To compensate for the results of the ideal equations and assumptions, the orifice discharge coefficient is introduced to account for the condition of the real flow that makes it non-ideal. The following equations are used to determine mass flow rate through a nozzle:

$$\dot{m} = C_d \rho_e A M_e c_e, \tag{3}$$

in which

$$M_e = \sqrt{2/(k-1)\left[(P_t/P_b)^{\left(k-\frac{1}{k}\right)} - 1\right]}, \tag{4}$$

$$T_e = \frac{T_t}{1+\frac{k-1}{2}M_e^2}; c_e = \left[\frac{kT_e\bar{R}}{MW}\right]^{1/2}; \rho_e = \frac{P_b}{\frac{T_e\bar{R}}{MW}}.$$

The coefficient discharge calculated by Equation (4) has the same result as Equation (2) if P_b is considered to be equal to p_2.

6.4. Temperature results

Table 4 shows a comparison between the main results of temperature by means of the numerical calculation and the experimental figures. Three different burner heat load conditions were analyzed. Predicted temperatures were higher than experimental temperatures. However, the differences are acceptable considering the purpose of this work.

Fig. 15a shows a vertical cross-section of the temperature contour along the furnace and Fig. 15b shows a horizontal cross section of the temperature contour. Fig. 15c shows a photograph of the flame at the same region indicated in Fig. 15a by a dashed line. This picture was taken from the slab entrance side. It can be noted that the shape of the simulated flame is very similar to the real one. It is not possible to show a picture of the entire flame because the slabs and the structural part of the skids interfere in direct view of the flame. However, the shape and length of the flame, as shown in Fig. 15a and b, seem to be fairly similar to the real flame for normal operation of the burner. Fig. 15b shows that the flame has a tendency to follow the streamline in the direction of the flare stack due to flue draft, noting that there is an equal opposite burner in the same direction.

7. Conclusion

As the design of an industrial fuel orifice is essential for a proper mix of fuel and combustion air, an approach that is also made up of the physical situation before the interaction between fuel and oxidizer can be very important to proper combustion modeling.

The flow through the burner nozzle has been simulated successfully using Fluent CFD code. There is satisfactory agreement between the numerical simulation predictions and experimental data and also between the numerical simulation predictions and practical approaches to burner scale. This validates the numerical results and also the applicability of the turbulence models tested. The k–ε (standard, RNG and Realizable) and RSM (Reynolds Stress Model) models provided good results, though the standard k–ε gave a slight different result from the others. The choice of the model becomes only a matter of computational power. The Realizable k–ε is recommended considering this point.

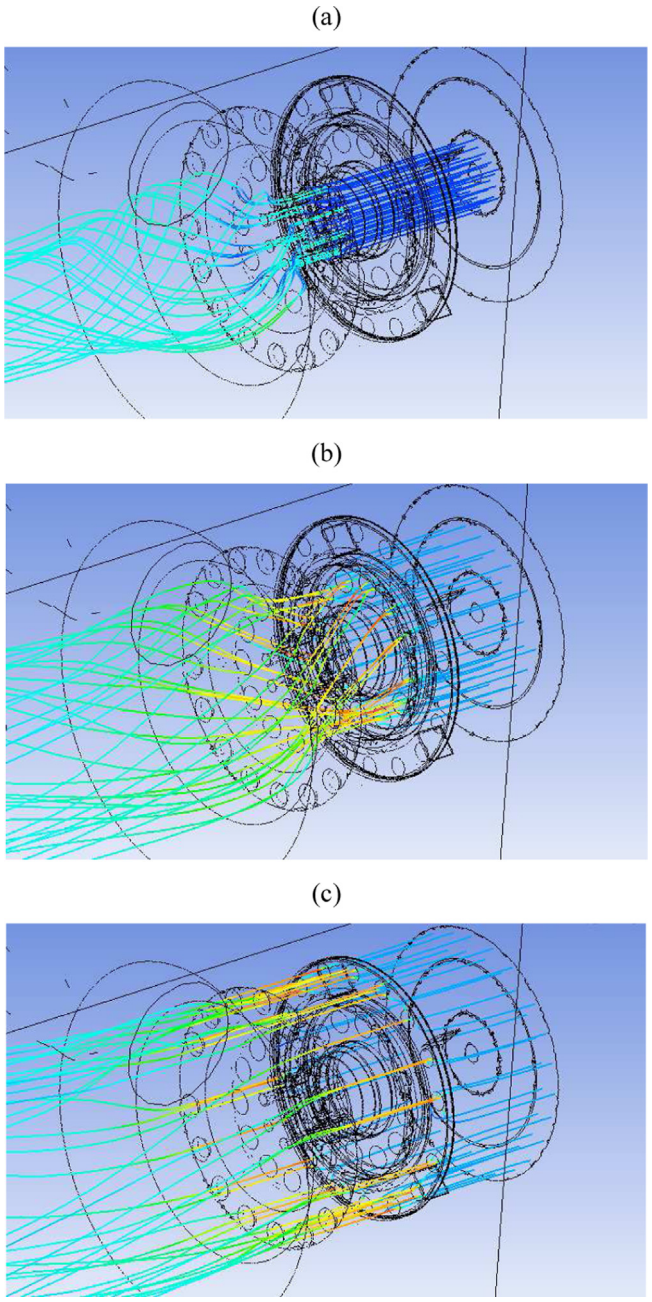

Fig. 10. Streamlines originating from natural gas nozzles (a), from primary combustion air nozzles (b), and from secondary combustion air nozzles (c).

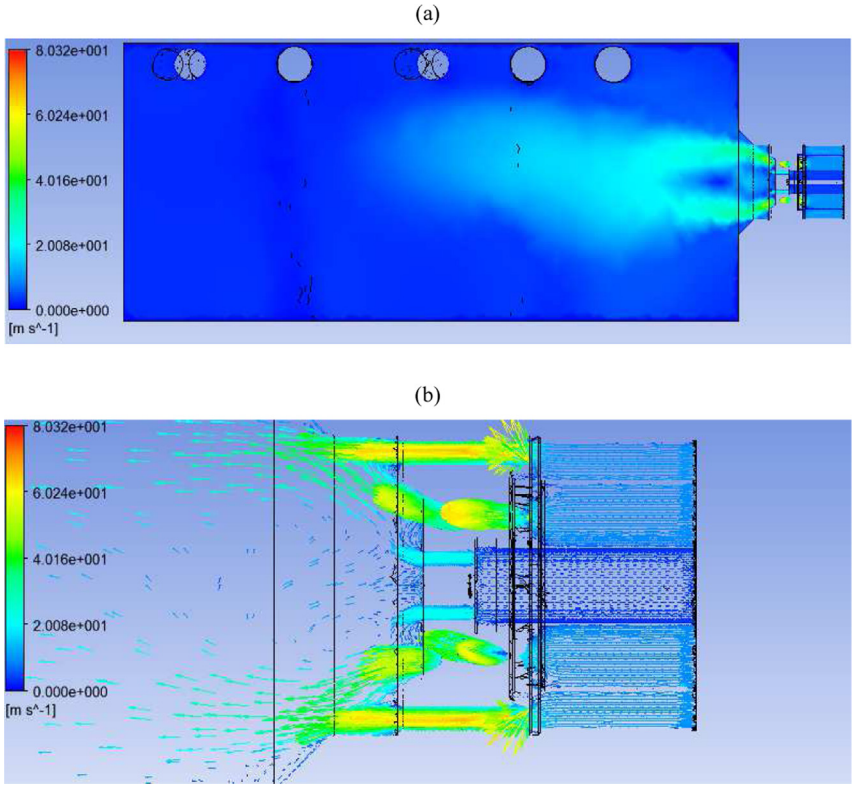

Fig. 11. Longitudinal cross-section of the burner/furnace: velocity contour (a), velocity vector (b).

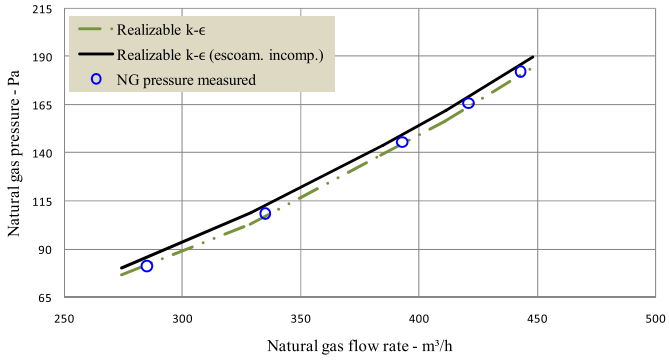

Fig. 12. Comparison between the results for incompressible and compressible flows.

It can be concluded that three dimensional numerical simulations are an effective tool to design burner nozzles and can give a more accurate burner design when used along with empirical or practical approaches, since it is able to give results showing complex situations in a very clear way and providing very valuable recommendations.

Industrial applications with respect combustion can be sensitive to changes in fuel gas quality. Particularly for steelworks, where besides natural gas other fuels are used, such as coke oven gas, blast furnace gas and steel plant gas. As those fuels are process waste gases, variation of the chemical composition is inherent to the process. Even for natural gas, nowadays there is a worldwide concern regarding gas quality and consequently gas interchangeability, due to composition variation, in view of cross-border transport of gas has increased a lot in recent years, and notably the rapid developing world market in liquefied natural gas. For industrial applications a typical variation in gas composition does not result in operation that causes the process unsafe or inoperable. However, there are potential negative changes with respect to

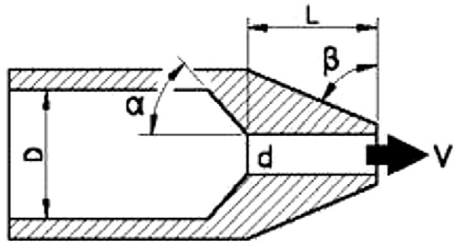

Fig. 13. Factors influencing the discharge coefficient (length-to-diameter ratio = L/d; beta ratio = d/D; port angle = α, exit angle = β).

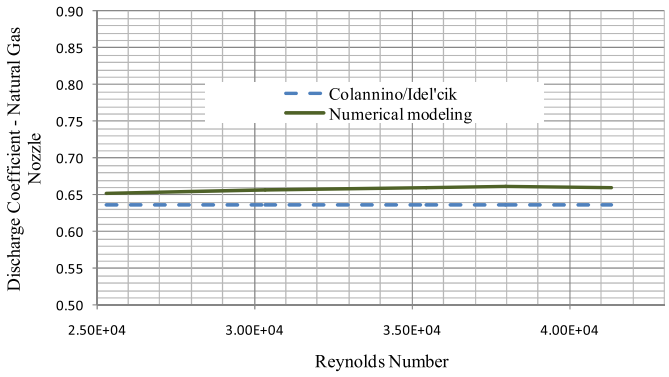

Fig. 14. Natural gas nozzle discharge coefficients for differential pressure (ΔP_{1-2}) from upstream from the nozzle to downstream from the nozzle as a function of Reynolds number.

Table 4
Comparison of experimental and simulated temperature values.

		Case#2 Burner load: 4,372 kW		Case#4 Burner load: 3,754 kW		Case#6 Burner load: 2,643 kW	
		Experimental	Simulation	Experimental	Simulation	Experimental	Simulation
$T_{furnace}$[a]	°C	1305	1343	1290	1331	1230	1297
T_{floor}	°C	1270	1275	1260	1274	1180	1267
$T_{slab\text{-}lower\ face}$	°C	985	1058	974	1058	926	1015
$T_{burner\ wall}$	°C	1270	1287	1260	1281	1180	1261

[a] Out of the flame.

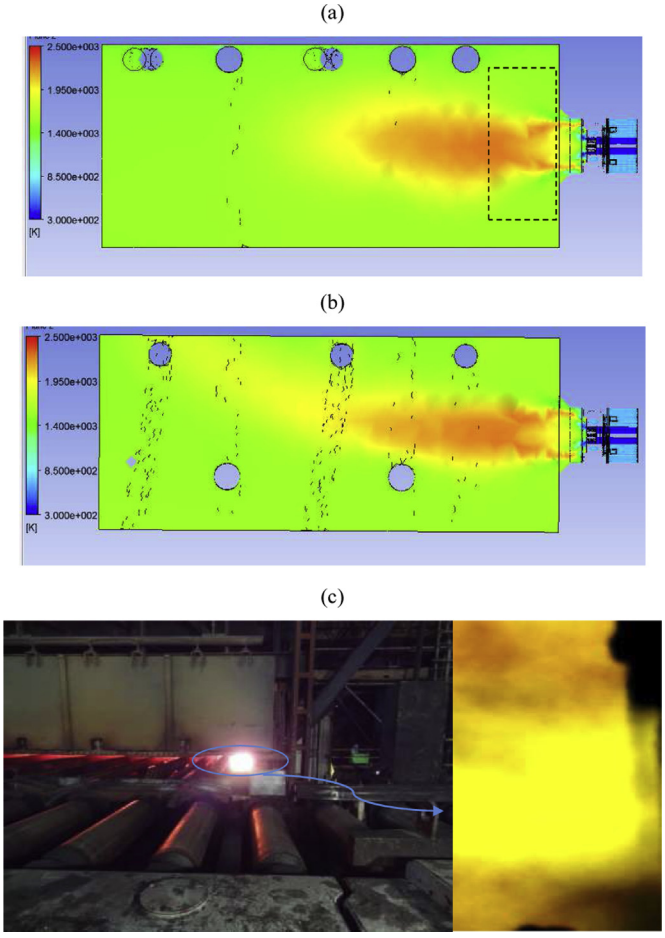

Fig. 15. Temperature contour along the furnace: vertical cross-section view (a), and horizontal cross-section view (b). Photograph of the flame in the region between the burner and the first skid (c).

emissions, efficiency and product quality. As an example, steel reheating furnaces require controlled atmosphere to maintain the oxygen in the flue gas under a close range, in order to ensure a proper scale formation on the metal surface. Therefore, the use of a numerical tool capable to redesign burner nozzles or to determine the correct pressure for an existing burner nozzle under operation, in case of a variation of fuel composition, is valuable to combustion performance. For the same fuel, when there is a decrease in the Wobbe Index, due to variation in gas composition, the only way to adjust the delivery of the same amount of heat is increasing the orifice upstream pressure. The Wobbe Index (WI) is a parameter of gas interchangeability and its usefulness is that for any given orifice, all gas mixtures that have the same WI will deliver the same amount of heat, at the same burner pressure. It is important to emphasize that in almost all gas appliances the flow gas is regulated by making it pass through an orifice.

Acknowledgements

The authors thank Companhia Siderúrgica Nacional (CSN) for allowing the use of its facilities and for technical support of operating personnel.

References

[1] M.S. Shah, J.B. Jyeshtharaj, S.K. Avtar, C.R.C. Prasad, D.S. Shukla, Analysis of flow through an orifice meter: CFD simulation, Chem. Eng. Sci. 71 (2012) 300–309.
[2] G.H. Nail, A Study of 3-Dimensional Flow through Orifice Meters, Ph.D. Dissertation, Texas A&M University, USA, 1991.
[3] G.L. Morrison, R.E. DeOtte, G.H. Nail, D.L. Panak, Mean velocity and turbulence fields inside a β = 0.50 orifice flowmeter, AIChE J. 39 (1993) 745–756.
[4] C.L. Hollingshead, M.C. Johnson, S.L. Barfuss, R.E. Spall, Discharge coefficient performance of Venturi, standard concentric orifice plate, V-cone and wedge flow meters at low Reynolds numbers, J. Pet. Sci. Eng. 78 (2011) 559–566.
[5] N.M.B. Oliveira, L.G.M. Vieira, J.J.R. Damasceno, Numerical methodology for orifice meter calibration, Mater. Sci. Forum 660–661 (2010) 531–536.
[6] S. Eiamsa-ard, A. Ridluan, P. Sumruasin, P. Eiasma-ard, P. Promvong, Numerical investigation of turbulent flow through a circular orifice, KMITL Sci. J. 8 (2008) 43–50.
[7] A. Erdal, H.I. Andersson, Numerical aspects of flow computation through orifices, Flow. Meas. Instrum. 8 (1997) 27–37.
[8] R.R. Rhinehart, S. Gebreyohannes, U.M. Sridhar, A. Patrachari, M.S. Rahaman, A power law approach to orifice flow rate calibration, ISA Trans. 50 (2011) 329–341.
[9] W. Borutzky, B. Barnard, J. Thoma, An orifice flow model for laminar and turbulent conditions, Simul. Model. Pract. Theory 20 (2002) 141–152.
[10] M. Reader-Harris, N. Barton, D. Hodges, The effect of contaminated orifice plates on the discharge coefficient, Flow. Meas. Instrum. 25 (2012) 2–7.
[11] A.E. German, T. Mahmud, Modelling of non-premixed swirl burner flows using a Reynolds-stress turbulence closure, Fuel 84 (2005) 583–594.
[12] A. Khelil, H. Naji, L. Loukarfi, G. Mompean, Prediction of a high swirled natural gas diffusion flame using a PDF model, Fuel 88 (2009) 374–381.
[13] K.M. Saqr, H.S. Aly, M.M. Sies, M.A. Wahid, Computational and experimental investigations of turbulent asymmetric vortex flames, Int. Commun. Heat Mass Transfer 38 (2011) 352–362.
[14] B. Danon, E.S. Cho, W. de Jong, D.J.E.M. Roekaerts, Numerical investigation of burner positioning effects in a multi-burner flameless combustion furnace, Appl. Therm. Eng. 31 (2011) 3885–3896.
[15] A.O. Nieckele, M.F. Naccache, M.S.P. Gomes, Combustion performance of an aluminum melting furnace operating with natural gas and liquid fuel, Appl. Therm. Eng. 31 (2011) 844–851.
[16] A. Frassoldati, P. Sharma, A. Cuoci, T. Faravelli, E. Ranzi, Kinetic and fluid dynamics modeling of methane/hydrogen jet flames in diluted coflow, Appl. Therm. Eng. 30 (2010) 376–383.
[17] M. Sarlej, P. Petr, J. Hájek, P. Stehlik, Computational support in experimental burner design optimization, Appl. Therm. Eng. 27 (2007) 2727–2731.
[18] K.M. Saqr, H.S. Aly, M.M. Sies, M.A. Wahid, Effect of free stream turbulence on NO_x and soot formation in turbulent diffusion CH_4 air flames, Int. Commun. Heat Mass Transfer 37 (2010) 611–617.
[19] K. Khanafer, S.M. Aithal, Fluid-dynamic and NO_x computation in swirl burners, Int. J. Heat Mass Transfer 54 (2011) 5030–5038.
[20] H.I. Kassem, K.M. Saqr, H.S. Aly, M.M. Sies, M.A. Wahid, Implementation of the eddy dissipation model of turbulent non-premixed combustion in OpenFOAM, Int. Commun. Heat Mass Transfer 38 (2011) 363–367.
[21] K.M. Saqr, M.A. Wahid, Comparison of four eddy-viscosity turbulence models in the eddy dissipation modeling of turbulent diffusion flames, Int. J. Appl. Math. Mech. 7 (2011) 1–18.

[22] T. Gassoumi, K. Guedri, R. Said, Numerical study of the swirl effect on a coaxial jet combustion flame including radiative heat transfer, Numer. Heat Transfer Part A 56 (2009) 897–913.
[23] M.D. Emami, A.E. Fard, Laminar flamelet modeling of a turbulent $CH_4/H_2/N_2$ jet diffusion flame using artificial neural networks, Appl. Math. Model. 36 (2012) 2082–2093.
[24] Fluent Inc., Fluent 12.0.12 User's Guide, 2009.
[25] B.E. Launder, D.B. Spalding, Mathematical Models of Turbulence, Academic Press, London, 1972.
[26] C.E. Baukal, Industrial Burner Handbook, CRC Press, USA, 2003.
[27] R. Aman, H. Handroos, T. Eskola, Computationally efficient two-regime flow orifice model for real-time simulation, Simul. Model. Pract. Theory 16 (2008) 945–961.
[28] J. Colannino, Modeling Combustion Systems: a Practical Approach, CRC Press, Taylor & Francis Group, USA, 2006.
[29] I.E. Idel'cik, Mémento de Pertes de Charges, Eyrolles. Collection de La Direction des Etudes etRecherchesd'Electricité de France, 1986.